Nanoscale

Accepted Manuscript

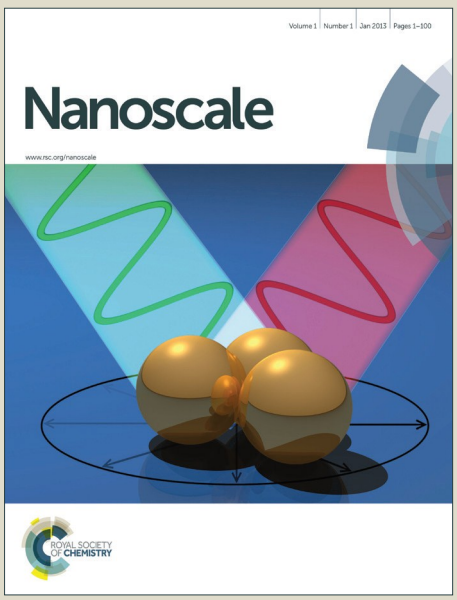

ROYAL SOCIETY OF CHEMISTRY

www.rsc.org/nanoscale

Nanoscale

PAPER

SERS activity with tenfold detection limit optimization on a type of nanoporous AAO-based complex multilayer substrate

Received 00th January 20xx,
Accepted 00th January 20xx

DOI: 10.1039/x0xx00000x

www.rsc.org/

Chaofan Sui,[ab] Kaige Wang,*[ab] Shuang Wang,[ab] Junying Ren,[a] Xiaohong Bai[c] and Jintao Bai[ab]

Most of SERS applications are constricted by heterogeneous hotspots and aggregates of nanostructure, which result in low sensitivity and poor reproducibility of characteristic signals. This work intends to introduce SERS properties of a type of SERS-active substrate, Au-$CuCl_2$-AAO, which is innovatively developed on a porous anodic alumina oxide (AAO) template. Spectral measuring results of Rhodamine 6G (R6G) on this substrate optimized by controlling morphology and gold thickness showed that enhancement factor (2.30×10^7) and detection limit (10^{-10} M) were both improved and represented better performance than its template AAO. Homogenous hot spots across the region of interest were achieved by scanning SERS intensity distribution for the band at 1505 cm^{-1} in 5×5 μm^2 area. Furthermore, the promising SERS activity of the flower-patterned substrate was theoretically explained through the simulation of electromagnetic field distribution. In addition, this SERS substrates is proposed for the applications within the field of chemical and biochemical analyses.

1. Introduction

Raman spectroscopy provides intrinsic fingerprint information by which the basic sample composition can be identified from a small scatter cross section.[1, 2] Since the dawn of Raman spectroscopy, its applications have been broadened in physical, chemical, biological and biomedical fields, but still restricted to weak signals. Until 1974, Fleishmann's group discovered that Raman signals could be enhanced when pyridine molecules adsorbed on the surface of electrochemically roughened Ag electrode,[3] which was defined as Surface Enhanced Raman Scattering (SERS) and opened a new period of Raman spectroscopy in the biochemical applications. As a noninvasive surface sensing technique and a powerful analytical tool, SERS mainly benefits from the enhanced local electromagnetic field of rough surfaces of Ag, Au, and Cu or specific metal-coated nanostructures excited by laser with appropriate wavelength.[4] It not only inherits the capability of Raman spectroscopy to provide molecular fingerprint information, but also enhances signal intensity with a unique molecular sensitivity.[5, 6] After decades of developments, its advantages have attracted a lot of interests in various fields, such as chemical system analysis, biomedical detection and environmental analysis, etc.[7-13]

In recent years, substantial works were conducted to promote the reliability of SERS. It is known that three major concerns for SERS-based label-free analysis of biochemical system are sensitivity, reproducibility and native state in practical applications. Generally speaking, the sensitivity mainly depends on the design and preparation methods of SERS-active nanostructure or nanoparticals,[14-18] such as sol-gel,[19] self-assembly,[20] E-beam Lithography (EBL),[21, 22] Focus Ion Beam (FIB),[23] nano-imprint lithography[24] and template technology.[25, 26] The EBL and FIB are ideal for producing uniform and reproducible SERS substrates enable reaching high enhancement factor, but are too expensive in mass production and infeasible to obtain large-scale nanostructures. Silver nanoparticles can reach to an extraordinarily high enhancement factor, however, they still suffer from aggregation state, which makes the results unreliable and difficult for standardization in different analytes production conditions.

Lately, it has been demonstrated that nano-material prepared by template synthesizing can provide good properties for SERS system,[27-29] since favourable uniformity of the prepared substrates are conductive to spectral investigation. Among them, porous anodic alumina oxide (AAO) film is one of the most widely used templates with nanochannels regularly arranged in honeycomb structure.[30-32] It has also been proved to be a large-area SERS-active device from experimental and theoretical aspects in recent works.[33-37] SERS based on AAO substrate has attracted amount of attentions for its effectiveness, controllability of various configuration shapes as well as simple preparation procedures. In 2009, Peter Nielsen achieved lowest detectable concentration limit ca. 10^{-9} M of R6G on Au-AAO substrate.[33] In 2010, Dukhyun Choi systematically studied and optimized the characterization of SERS responses by controlling gold thickness and AAO thickness, and the enhancement factor (EF) of the substrate was achieved to 8.1×10^6.[34] And more recently in 2014, Kamilla Malek obtained

[a] National Key Laboratory Base of Photoelectric Technology & Functional Materials Co-sponsored by Province and Ministry, Institute of Photonics & Photon-Technology, Northwest University, Xi'an, 710069, China. E-mail: wangkg@nwu.edu.cn
[b] International technology cooperation base of Photoelectric technology and functional materials of Ministry of science and technology, Northwest University, Xi'an, 710069, China.
[c] Xi'an Institute of Optics & Precision Mechanics Chinese Academy of Science, Key Laboratory of Ultrafast Photoelectric Dignostic Technology, Xi'an, 710119, China.

high-resolution SERS imaging instead of single-point measurements to investigate intensity distributions of characteristic peaks and the effect of nanostructure based on Au-AAO substrate.[36]

In this work, we developed a type of large-area flower-patterned nanostructure, Au-$CuCl_2$-AAO, which is self-assembled on AAO template via a simple, economical, but effective improving treatment and capable of measuring high quality SERS spectra of R6G. By measuring SERS spectra of probe on substrates with various morphologies and depositing different gold thicknesses, the optimal structure suitable for SERS was designed. The detectable concentration limit was broke through on the optimal substrate, which was lower than that on AAO substrate, and the enhancement factors of each characteristic peak were evaluated.[33] Other SERS properties such as reproducibility and uniformity have also been investigated to prove its potential in practical applications. Moreover, distributions of three-dimension electric fields in Au-AAO and Au-$CuCl_2$-AAO substrates excited by plane waves with different polarizations were theoretically calculated to explain this enhancement mechanism.

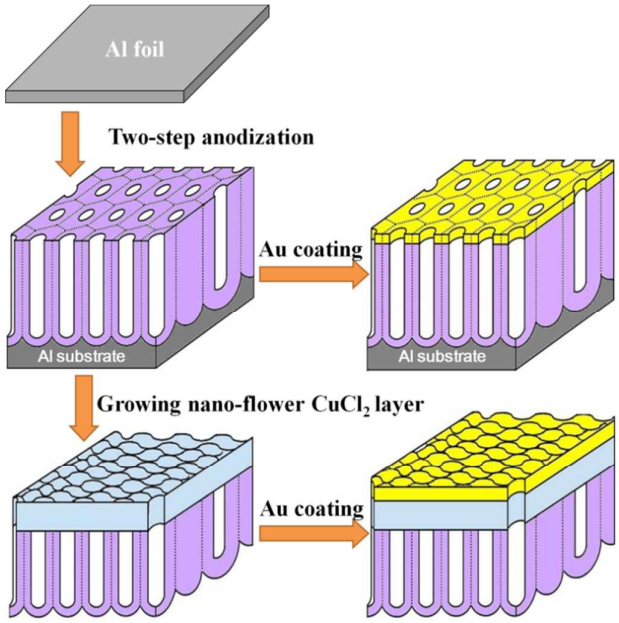

Fig. 1 Preparation processes of two nanostructured SERS-active substrates.

2. Experimental

2.1 Materials

Aluminum foils (99.999%) were purchased from General Research Institute for Nonferrous Metals, Beijing, China. Anhydrous alcohol, acetone, chromic acid (H_2CrO_4), sulfuric acid (H_2SO_4), phosphoric acid (H_3PO_4) and oxalic acid ($C_2H_2O_4$) were purchased from Hedong Red Cliff Chemical Reagent Factory, Tianjin, China. Copper chloride dehydrate ($CuCl_2 \cdot H_2O$) was purchased from Guanghua chemical factory Co., Ltd, Guangdong, China. All chemicals were of analytical grade purity and used as received without further purification.

2.2 Substrate fabrication

The brief preparation processes of Au-AAO and Au-$CuCl_2$-AAO substrates are shown in Fig. 1. The AAO templates were fabricated with standard two-step anodic oxidation method. Before fabrication, ultrapure aluminum foils were annealed (500 °C, 5h) in vacuum tube furnace to increase the number of lattices and relieve inside stress. After the surface native oxidation layer was removed, anodic oxidation processes were carried out at 0 °C and 40 V voltages in 0.3 M $C_2H_2O_4$ electrolyte. Finally, samples were immersed in 3 wt.% H_3PO_4 for holes expanding to achieve better uniformity.

The home-made Au-$CuCl_2$-AAO substrate a multilayer "flower-pattern" nanostructure grown on the AAO template via self-assembly method. AAO templates were soaked in 2.48 M $CuCl_2$ aqueous solution to remove Al substrates, and then rinsed with sufficient deionized water (Heal Force, China) until surface contaminants were completely cleaned. Finally, a few drops of $CuCl_2$ solution with specific concentration were added onto a template, and samples were subsequently stored at a certain temperature. The final formed morphology depends on a variety of factors. Among them, three of the most pivotal experimental conditions are temperature, concentration of $CuCl_2$ solution and sample storage time. More detailed fabrication processes and growth mechanism about the $CuCl_2$-AAO nanoflower layer will be introduced elsewhere.

In order to use these nanostructures as SERS-active substrates, thin gold layers were thermally evaporated onto all substrates using customized vacuum thermal evaporator. Surface morphologies were characterized using field emission scanning electron microscope (FE-SEM, SU8010, Hitachi) with a maximum resolution of 1 nm at 15 kV.

2.3 SERS measurements

Rhodamine 6G (R6G, Aladdin Industrial Corporation, China) aqueous solution was employed as probe molecule due to its high adsorption energy yielded Raman enhancement and ability to retain its native state.[38] SERS measurements were carried out after probe solution quantificationally dropped onto substrates, and dried at room temperature to ensure molecules were adsorbed completely.

The experimental procedures can be briefly described as follows: firstly, for comparing the Raman spectra of R6G collected from different substrates with at same conditions, 1 μM probe solution was dropped directly onto substrates, and 100mM probe solution was dropped on the quartz plate as a reference to calculate enhancement factors of each SERS band; secondly, three-time cumulative average spectra at 10 randomly selected spots were measured in 5s integration time to verify reproducibility and reliability; thirdly, in order to examine the uniformity of Au-$CuCl_2$-AAO substrate, SERS scanning was

performed through 5×5 μm^2 area (120×120 pixels) in 1s integration time at each pixel without cumulation among a single substrate to obtain SERS intensity distribution in the interested area; finally, concentration of R6G solution was reduced regularly in ten percent till Raman signals disappeared to obtain the lowest detectable concentration of probe solution.

Considering that fluorescence excitation wavelength of R6G is from 200 to 530 nm, a 633 nm laser was chosen as excitation source. SERS spectra measurements were carried out by using Alpha 500R Confocal Raman Microscopy System (WITec, German) equipped with a 633 nm laser (beam size: ca. 1μm using a 100×, NA=1.2 objective) and a EMCCD (UHTS 300). The greatest advantages of this instrument are the capabilities of superfast spectral measuring and high-resolution imaging, by which matter distribution would be discerned using three dimensional scanning combined with "finger-print" recognition function of Raman spectroscopy on the same equipment. SERS spectra were collected in a range of Raman shifts from 0 to 2750 cm^{-1} with a 600 g/mm grating. All of the measured spectra were processed by means of a system supporting software, WITec Project Four.

3. Results and discussion

3.1 Surface morphology of AAO and $CuCl_2$-AAO substrates

Fig. 2i(a) and 2i(b) show the top-view and cross-section SEM images of as-prepared $CuCl_2$-AAO film, respectively. The nanostructure is composed of "nanoflowers" with petal length of ca. 200 nm and petal thickness of ca. 20-30 nm. Three or four "nanopetals" are basically grown from each intersection. The profile presents obvious roughness on the surface. The thickness between the spot, i.e. the aforementioned intersection and AAO surface is ca. 317 nm. In spite of these irregular shape cells, the distribution of nanoflowers is homogeneous in appearance morphology viewed as a whole.

Some other typical surface morphologies of $CuCl_2$-AAO nanostructures prepared under different conditions and failed to grow large-area nanoflowers were provided in Fig. 2i(c)-(g). By decreasing storage time to 1 day but maintaining concentration of $CuCl_2$ solution and temperature conditions, most nanopores began to be coated with small pieces as shown in Fig. 2i(c). From Fig. 2i(d), the generated morphology is the result of baking the substrate in oven to hasten the drying process. However, shape of nanopetals became more wrinkled and irregular during annealing. The nanostructure shown in Fig. 2i(e) was prepared by dropping saturated $CuCl_2$ solution and stord at 5 °C, nanopores were completely covered by the formed material. After bonding with water molecules, excessive $CuCl_2 \cdot H_2O$ molecules aggregated and accumulated together to generate bulks. The nanostucture in Fig. 2i(f) was prepared using 81.947 mg/L $CuCl_2$ solution. The nanostructure in Fig 2i(g) was prepared using 11.815 mg/L $CuCl_2$ solution and stored in an incubator chamber at 5 °C for 7 days, which shows sporadic particles and exposed nanopores of AAO layer below. It was speculated that the number of $CuCl_2$ molecules within a unit volume were too few to form clusters. All the analysis suggested that the concentration being excessively high or low, and incorrect storage time, etc., cannot produce the

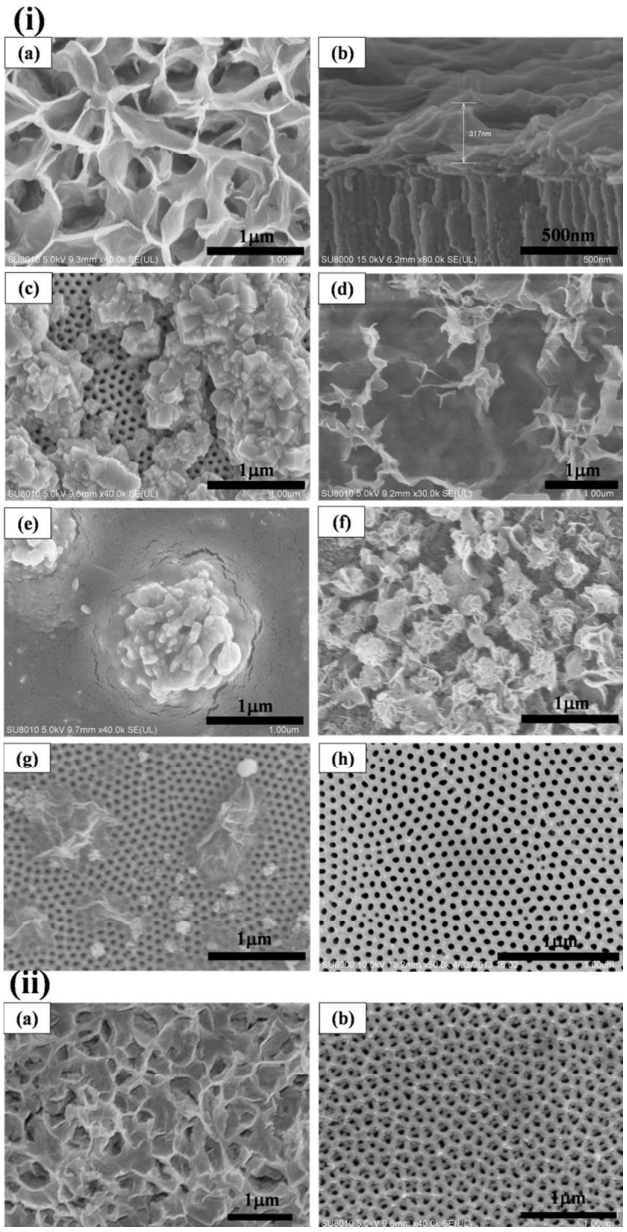

Fig. 2 (i) SEM images of nanostructures fabricated under different conditions. (a)-(g) $CuCl_2$-AAO: (a) 27.15 mg/L $CuCl_2$ solution, stored at room temperature for 7 days (top-view image); (b) the profile of the sample as shown in (a); (c) 27.15 mg/L $CuCl_2$ solution, stored at room temperature for 12 h; (d) 27.15 mg/L $CuCl_2$ solution, dried in oven for 5h; (e) saturated $CuCl_2$ solution, stored at 5 °C for 7 days; (f) 81.947 mg/L $CuCl_2$ solution, stored at room temperature for 7 days. (g) 11.815mg/L $CuCl_2$ solution, stored at room temperature for 7 days; (h) AAO. (ii) SEM images of substrates after 25nm gold coated: (a) Au-$CuCl_2$-AAO; (b) Au-AAO.

ideal structure. Based on extensive testing, the most ideal nanostructure was fabricated under $CuCl_2$ concentration within the range of 25 to 30 mg/L and incubating time of 7 days.

From the Fig. 1i(h), AAO substrate is apparently observed in an excellent uniform structure, in which pores are mainly arranged in the centres of each hexagonal cell by an ordered manner. The average pore size is evaluated to be ca. 60 nm; wall thickness between pores is ca. 40 nm, which means the size of each cell is ca. 100 nm decided by its intrinsic properties.

Fig. 2ii shows SEM images of $CuCl_2$-AAO and AAO substrates after 25nm gold coated. Under uniform coating condition, morphology of $CuCl_2$-AAO substrate was nearly unchanged, but gold piling up on edges of nanopetals has made the petals thicker. On Au-AAO substrate, gold mainly piled up on sides of hexagonal units because of small-size pores.

3.2 SERS measurements on substrates with different structures

Fig. 3i shows spectra of 1μM R6G absorbed on Au-$CuCl_2$-AAO, Au-AAO and Al substrates corresponding to lines in black, red and blue, respectively. Characteristic peaks of R6G are exhibited at 608, 772, 1187, 1313, 1363, 1505, 1572, 1599 and 1645 cm^{-1}, which are attributed to vibrational modes ν_{53}, ν_{65}, ν_{105}, ν_{115}, ν_{117}, ν_{146}, ν_{147}, ν_{151}, and ν_{154},[41] respectively. Among them, ν_{53} and ν_{151} correspond to C-H in-plane deformation of the xanthene ring and C=C symmetric stretching motion, respectively. R6G bands at 772, 1187, 1313 cm^{-1} are attributed to C-H wagging vibration while bands at 1363, 1505 and 1645 cm^{-1} are attributed to C=C totally symmetric stretch of the xanthene ring, respectively. Interaction between R6G molecule and metal surface results in elongation of aromatic nucleus, which renders the appearance of the weak peak at 1572 cm^{-1} attributed to C=O stretching vibration of the benzene ring.

Comparing the recorded spectra in Fig. 3i, Raman signals were too weak to be detected on Al sheet while the strongest spectral intensity was achieved on Au-$CuCl_2$-AAO substrate, whose intensity is about four times higher than that on Au-AAO substrate. It can also be found that there are no obvious Raman frequency shift between corresponding peaks in spectra of two kinds of substrates, but intensity ratio of SERS bands at 1599 and 1645 cm^{-1} to other bands is observed stronger on Au-$CuCl_2$-AAO substrate than that on Au-AAO substrate. On the basis of physical enhancement mechanism in SERS studies, the enhancing effects for each peak should be equal; however, the experimental results are not conform (Fig. 3i). It can be reasonably speculated that chemical enhancement has made this contribution to the result that chemical reactions between adsorbate and metal surface increased molecular polarizability of R6G to increase the Raman scattering cross section. It has been demonstrated that formation of chemical bonds between metal surface and adsorbate will result in frequency shifts with respect to conventional Raman spectra and alteration of relative intensity between peaks. Chemical bonds formed between R6G molecules and Au-$CuCl_2$-AAO are distinguished from those between R6G molecules and Au-AAO substrate in bond energy

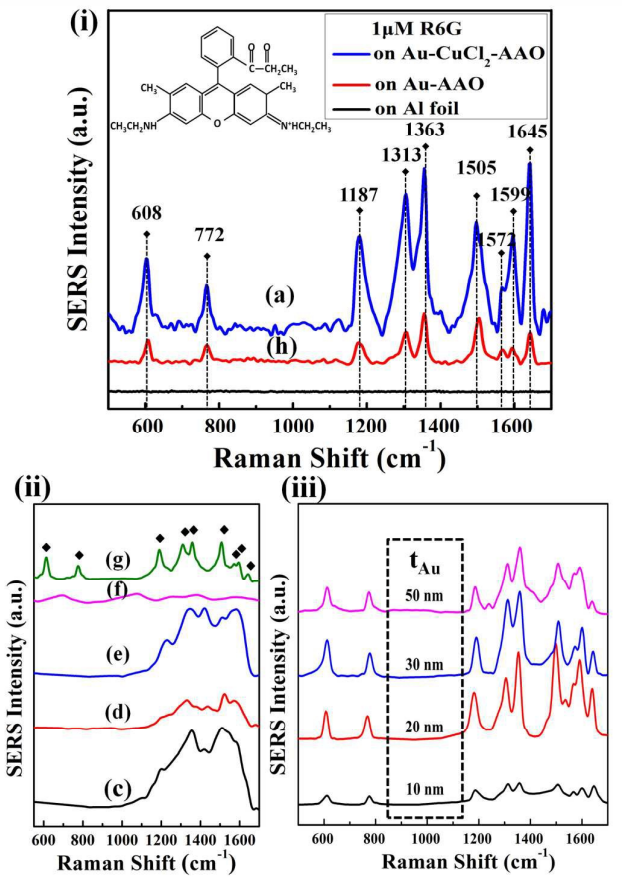

Fig. 3 SERS spectra of R6G on different substrates: (i) Al substrate (black), Au-AAO substrate (red) and Au-$CuCl_2$ substrate (blue), the inset is the molecular formula of R6G; (ii) Substrates failed to generate nanoflowers; (iii) Tunability of SERS spectra according to Au thickness from 10 to 50 nm in Au-$CuCl_2$-AAO substrate. The target molecule was 1 μM R6G.

and bond vibration amplitude, which explained the distinction of relative intensity between peaks.[39]

It is well-known that SERS effect mainly depends on the adsorbate, excitation frequency, shape of substrate and optical properties of surface metal. In this measurement, except for shape and gold thickness, other conditions were solid. Therefore, these two factors dominate the final enhancement effect. In order to determine the most effective structure for SERS, spectral measurements of 1 μM R6G were executed on above-mentioned substrates (Fig. 3c-3g) with 25 nm gold coated (Fig. 3ii). Among them, obvious SERS bands were only obtained on the substrate (g) as shown in Fig. 3g, which basically was, however, the contribution of exposed nanopores in AAO. Unlike gold-coated nanoflower structure, it was confirmed that none of substrates with irregular shapes on the surface (Fig. 3ii, c-f) was capable of enhancing Raman signals. Therefore, the flower-patterned structure is most effective for SERS among all these substrates on the structural side.

In addition to the aforementioned parameters, our substrate

was further optimized by changing gold thickness of 10, 20, 30 and 50 nm, respectively. SERS measurements were performed on the optimal shape. In Fig. 3iii, the strongest intensity was achieved on the substrate with 20-nm Au coated, next was the substrate with 30-nm Au. Based on extensive measurements, we drew a conclusion that the best design calls for the gold thickness between 20~30 nm.

3.3 SERS properties of the optimized Au-$CuCl_2$-AAO substrate

3.3.1 Sensitivity. Concentration of R6G was decreased order by order with a view to achieving the lowest detectable limit. Spectra are shown in Fig. 4. With concentration gradually decreased from 10^{-6} to 10^{-8} M, as shown in Fig. 4a, there is no obvious variation observed besides peak intensity. The most astonishing result is that the lowest detectable concentration achieved on Au-$CuCl_2$-AAO substrate, 10^{-10} M, has broken through that of the Au-AAO substrate by tenfold.[33] This substrate with such a commendable sensitivity was even favourably compared with current advanced solid SERS-active substrates fabrication technologies.[40-42]

Moreover, from the Fig. 4b, it can be noticed that the spectral line shape of R6G obviously alters comparing with preceding results when concentration decreases down from 10^{-9} M, while an envelope curve unexpectedly appears below SERS bands between 1200~1650 cm^{-1}. Despite an apparent impact of substrates' background on Raman spectral line shape, several characteristic peaks at 1313, 1363, 1572 and 1599 cm^{-1} are still able to be recognized. This phenomenon can be comprehended from two aspects. On the one hand, it can be explained by the effect of Localized Surface Plasmon Resonance (LSPR). When the strongest effect occurs at total reflection of incident light, the evanescent wave will rapidly decay far from the interface and the incident point within the distance on an order of the wavelength in a vertical direction, and half an order in an horizontal direction,[43] respectively. Since the distance between incident point and $CuCl_2$ layer is far less than the wavelength, it is reasonably assumed that the evanescent wave must have reached the $CuCl_2$ layer, which means Raman signals of R6G was definitely influenced by background signals of $CuCl_2$ layer. On the other hand, the appearance of SERS is always accompanied with fluorescence quenching phenomenon as a result of the chemical bonds formed between substrate and adsorbate.[44] Nonethless, the number of these corresponding chemical bonds can be reduced in consequence of lower density of R6G molecules at low concentration, which means the fluorescence quenching is also sharply weakened. Sequentially, background of substrate severely interfered with Raman signal when the concentration was lower than a certain threshold.

To determine SERS enhancement factors (EFs), R6G with a higher concentration of 100 mM was used due to the extremely weak intensity of the conventional Raman scattering. Normal Raman and SERS signals of R6G collected from the quartz substrate and 25 nm-gold coated substrate were measured (Fig. S1), respectively. SERS EFs are shown in the inset. As a result, the maximum EF is 2.30×10^7 at a Raman shift of 1363 cm^{-1}.

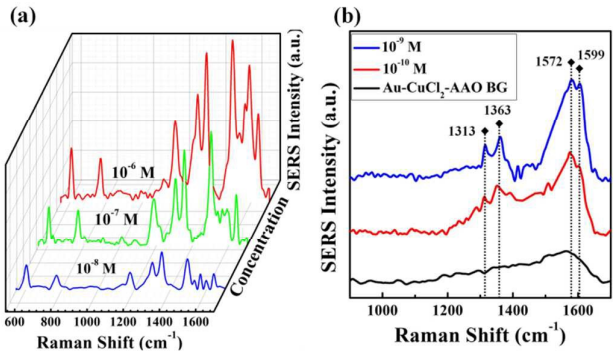

Fig. 4 States of changes in spectra over concentration of probe solution on Au-$CuCl_2$-AAO substrate: (a) concentration range from 10^{-6}-10^{-8} M; (b) The contrast of SERS spectra of 10^{-9} M (blue) and 10^{-10} M (red) R6G solution, as well as background of the substrate (black).

In addition, based on the SEM images of two substrates in Fig. 2, the proposed surface morphology have obviously larger surface area than that of Au-AAO which has numerous pores, which would have made a certain contribution to the enhancement. Thus, the surface area of Au-$CuCl_2$-AAO substrate was measured by AFM measurement(Fig. S2). The result shows that the surface area of Au-$CuCl_2$-AAO is 209 μm^2 at 100 μm^2 projected area The roughness factor is 2.09 while that for Au-AAO were reported to be 1.03 before.[45] Since the roughness factor is the ratio of surface area to projected surface area, the roughness factor ratio between two substrates (ca. 2.03) is equal to surface area ratio. For the same probe molecule, this ratio is also equal to the ratio of the number of absorbed molecules under identical measuring conditions. Therefore, the surface area increase do make a certain contribution to signal enhancement.

3.3.2 Reproducibility. In order to examine the reproducibility

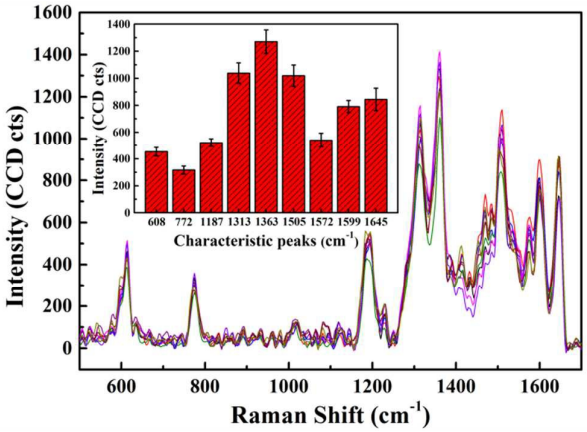

Fig. 5 SERS spectra of 1 μM R6G aqueous solution collected from 10 different spots on Au-$CuCl_2$-AAO substrate. The inset is mean ± standard deviation of Raman intensity for each characteristic peak.

of Au-$CuCl_2$-AAO substrate, 10 differently-located spots were randomly selected on a single substrate to measure spectra of 1μM R6G under the same conditions. The results are shown in Fig. 5. Mean values and standard deviations of SERS intensity for each characteristic peak were counted and shown in the inset. It is observed that all of the deviations are below 5%, which means our substrate is commendable and suitable for SERS applications with excellent reproducibility.

3.3.3 Homogeneity. To illustrate homogeneity of substrates, Raman signal intensity distribution of 1505 cm^{-1} through 5×5 μm^2 area was scanned by dropping 1μM R6G on single Au-$CuCl_2$-AAO substrate. The Raman image is shown in Fig. 6a and b, in which brighter spots represent higher intensity of corresponding bands generally called hot spots in SERS studies. On the top and bottom of the color scale, yellow and black represent the strongest and the weakest Raman signal across the entire region, respectively. In the Fig. 6a, Intensity recorded on this substrate shows a relatively homogeneous distribution of abundant hot spots in a large area, manifesting an admirable uniformity across the substrate. However, it can also be noticed that a number of black spots in weakest intensity obviously occur at the right bottom half of image. All of these spots with weakest intensity may originate from the collapse of structure when gold layer were thermally evaporated, which is not representative. The intensity distributions of other bands are similar with the shown one on the whole, some of subtle differences may stem from the oriented adsorption of R6G molecule. For instance, the integral electric field intensity of the peak at 1645 cm^{-1} is weaker than the shown one. Though they are attributed to similar vibrational modes, whose benzene ring in the molecular structure is adsorbed easily on the surface, and restricted symmetric stretch of C=O bonds at different position to some extents. In order to perform more detailed analyses, 2×2 μm^2 area (Fig. 6b) and a cross-section plot (Fig. 6c) were selected and marked in the Fig. 8a, by which the homogeneity of signals on Au-$CuCl_2$-AAO substrate can be observed more clearly.

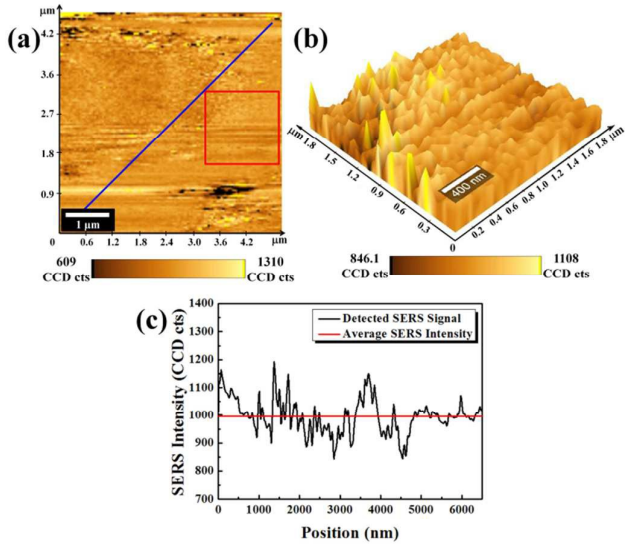

Fig. 6 (a) SERS intensity distribution for 1505 cm^{-1} band recorded on Au-$CuCl_2$-AAO substrate in 5×5 μm^2 area. (b) Intensity topography collected after SERS mapping through a 2×2 μm^2 region selected from the previous area marked in the (a). (c) Cross-section plot of the region labeled in the (a).

3.4 Distribution of electromagnetic fields

Theoretical models of both substrates were built under the conditions same as experiments. Three-dimension electric fields excited by plane waves with different polarizations were simulated using Finite Integration Technique (FIT). To deal with complex geometrical shapes, FIT is more beneficial than other methods such as FDTD to offer accurate approximate boundary condition. In fact, similar simulation method used on Au-AAO substrate has been done by other research groups to get more comprehensive understanding of enhancement effect.[35, 46] However, their simulation results were limited to a general distribution of electric field because the models were too crude, such as the nano-tips at the intersections of sides which are crucial for SERS were neglected.

During modeling, the inevitable alteration of pore size in gold layer from AAO channel diameter was considered.[47] AAO thickness, barrier layer thickness in AAO and gold layer thickness were set to be 500nm, 25 nm, 25nm, respectively, as well as the side length of hexagon, channel diameter and pore diameter in gold layer were 40nm, 60 nm and 55 nm, respectively. The excitation light source was a plane wave with a wavelength of 633 nm, polarized along x axis and propagating along the negative z axis. The amplitude of incident plane wave was always set to be 1 V/m.

Fig. 7 shows representative results of electric field intensity distributions of two substrates excited by plane waves polarized along x (Fig. 7a and 7b)) and y axis (Fig. 7c and 7d), respectively; the front and perspective images are both depicted. It can be noticed that strong electric fields mainly distribute at gold layers, especially on the metal surface, whereas field intensity values are very small and even are almost zero under gold layers. Field intensity values at every raised edge are higher than those on other regions and maximum values especially appear at the points where the lines intersect, which is attributed to the higher charge density at the part with bigger curvature. In addition, it is worth noting that polarization direction of excited light has certain impact on electric field intensity at hot spot and distribution. The incident light polarized along y axis excite stronger electric field. For polarized light P, the component perpendicular to the interface is the main cause acting on charges near interface. The coupling effect of nanostructure in polarization direction of incident electric field is much stronger than that in an orthogonal direction.

For a quantitative and more intuitive comparison, maximum values of electric fields intensity of gold layers on two substrates were calculated; the statistic data are shown in Table 1. By noticing that, the maximum value of electric field

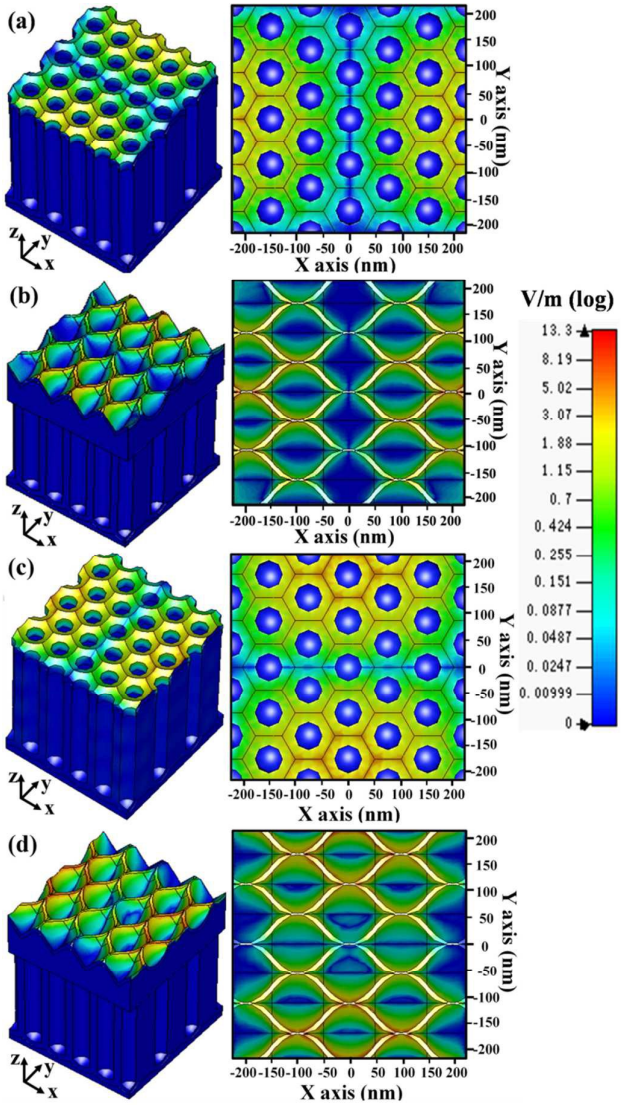

Fig. 7 Simulated 3D electric fields of Au-AAO and Au-$CuCl_2$-AAO substrates excited by incident light polarized along different direction: (a)(b) x axis; (c)(d) y axis.

intensity was achieved on Au-$CuCl_2$-AAO (13.349 V/m) when incident light polarized along y axis, which is about 2.11 times stronger than that of Au-AAO (6.3256 V/m). According to the electromagnetic mechanism, EM enhancement factor is the ratio of electric field intensity at hot spot (E) to the initial field (E_0) to the forth power as follow:

$$EF_{EM} = \left|\frac{E}{E_0}\right|^4 .$$

EF_{EM}s of two substrates were also calculated and shown in Table 1. Besides electric field, on the contrary, magnetic field has weakening effect on the enhancement.[48] Mean values of magnetic field intensity on two substrates were also counted , where magnetic field on Au-$CuCl_2$-AAO is always weaker than that on Au-AAO substrate no matter what direction the incident light was polarized along. Therefore, the results bring a better effect to SERS.

Table 1 Statistic data of simulated electric and magnetic fields of gold layers.

Polari-zation	Substrate	Maximum Electric field intensity (V/m)	EF_{EM}	Average Magnetic field intensity (A/m)
x	Au-AAO	6.1810	1.46×10^3	1.36×10^{-3}
	Au-$CuCl_2$-AAO	10.9742	1.45×10^4	1.23×10^{-3}
y	Au-AAO	6.3256	1.60×10^3	1.42×10^{-3}
	Au-$CuCl_2$-AAO	13.3490	4.19×10^4	1.33×10^{-3}

Above all, the simulation results not only theoretically explained mechanism of our substrates, but also suggested the stronger enhancement of Au-$CuCl_2$-AAO substrate, which is in accordance with experimental results.

4. Conclusions

In this work, the flower-patterned nanostructure, Au-$CuCl_2$-AAO, has been demonstrated to be a promising SERS-active substrate by multiple sets of experiments and simulations. Taking Au-AAO substrates as the reference, spectra of R6G collected on both substrates under the same experimental conditions indicated that this substrate is capable of reaching higher enhancement factor of 2.30×10^7 and lower detectable molar concentration limit at 10^{-10} M, which is tenfold improved on Au-AAO substrate. While sensitivity was improved, fairly high homogeneity in 5×5 μm^2 areas and excellent reproducibility were achieved, and merits of AAO template such as controllable large area were also inherited. In addition, the mechanism of this nanostructure was further clarified by simulation of electromagnetic fields based on FIT and numerical results. All of these properties mentioned above make the Au-$CuCl_2$-AAO substrate as an effective SERS substrate which can be practically applied in detecting single biomolecule in future works.

Acknowledgements

This project is supported by the National Natural Science Foundation of China (Grant No. 61378083, 11404258), the International Cooperation Foundation of the National Science and Technology Major Project of the Ministry of Science and Technology of China (Grant No.2011DFA12220), the Major Research Plan of the National Natural Science Foundation of China (Grant No. 91123030), and the Natural Science Foundation of Shaanxi Province of China (Grant No. 2010JS110, 2013SZS03-Z01, 2014JQ1011).

References

1. K. E. Shafer-Peltier, C. L. Haynes, M. R. Glucksberg and R. P. V. Duyne, *J.am.chem.soc*, 2003, **125**, : e20639.
2. K. Kneipp, H. Kneipp, G. Deinum, I. Itzkan, R. R. Dasari and M. S. Feld, *Applied Spectroscopy*, 1998, **volume 52**, 175-178(174).
3. M. Fleischmann, P. J. Hendra and A. J. McQuillan, *Chemical Physics Letters*, 1974, **26**, 163–166.
4. D. L. Jeanmaire and R. P. V. Duyne, *Journal of Electroanalytical Chemistry and Interfacial Electrochemistry*, 1977, **84**, 1–20.
5. M. Kerker, *Applied Optics*, 1980, **19**, 3373-3388.
6. R. Dornhaus, M. B. Long, R. E. Benner and R. K. Chang, *Surface Science Letters*, 1980, **93**, 240–262.
7. M. Sanles-Sobrido, *Nanoscale*, 2009, **1**, 153-158.
8. S. W. Bishnoi, Y. J. Lin, M. Tibudan, Y. Huang, M. Nakaema, V. Swarup, T. A. Keiderling and A. Chem., *Analytical Chemistry*, 2011, **83**, 4053-4060.
9. Q. XM, *Chem Soc Rev*, 2008, **37**, 912-920.
10. G. Das, F. Mecarini, F. Gentile, F. D. Angelis, H. M. Kumar, P. Candeloro, C. Liberale, G. Cuda and E. D. Fabrizio, *Biosens Bioelectron*, 2009, **24**, 1693–1699.
11. A. Singh, M. Chaudhari and M. Sastry, *Nanotechnology*, 2399, **17**, 2399-2405.
12. J. Qi, J. Zeng, F. Zhao, S. H. Lin, B. Raja, U. Strych, R. C. Willson and S. Wc., *Nanoscale*, 2014, **6**, 8521-8526.
13. S. Lee, H. Chon, S. Y. Yoon, E. K. Lee, S. I. Chang, D. W. Lim and J. Choo, *Nanoscale*, 2012, **4**, 124-129.
14. K. Kneipp, Y. Wang, H. Kneipp, L. T. Perelman, I. Itzkan, R. R. Dasari and M. S. Feld, *Physical Review Letters*, 1997, **78**, 1667-1670.
15. L. JF, H. YF, D. Y, Y. ZL, L. SB, Z. XS, F. FR, Z. W, Z. ZY and W. d. Y, *Nature*, 2010, **464**, 392-395.
16. J. Fang*†§, S. Du‡, S. Lebedkin§, Z. Li‡ and R. Kruk, *Nano letters*, 2010, **10**, 5006-5013.
17. J. Theiss, P. Pavaskar, P. M. Echternach, R. E. Muller and S. B. Cronin, *Nano Lett*, 2010, **10**, 2749-2754.
18. J. Xian, L. Chen, H. Niu, J. Qu and J. Song, *Nanoscale*, 2014, **6**, 13994-14001.
19. S. Lucht, T. Murphy, H. Schmidt and H. D. Kronfeldt, *Journal of Raman Spectroscopy*, 2000, **31**, 1017–1022.
20. L. Polavarapu and Q. H. Xu, *Langmuir*, 2008, **24**, 10608-10611.
21. W. SM, R. SD, O. JM and S. MJ., *ACS Nano*, 2009.
22. L. YY, L. JD, Y. ML and W. CL., *Biosensors & bioelectronics*, 2012, **35**, 447–451.
23. M. Qiao, M. J. L. Santos, E. M. Girotto, A. G. Brolo and R. Gordon, *J.phys.chem.c*, 2008, **112**, 15098-15101.
24. S. Krishnamoorthy, S. Krishnan, P. Thoniyot and Y. L. Hong, *Acs Applied Materials & Interfaces*, 2011, **3**, 1033-1040.
25. L. U. Yu-Dong, X. Q. Ren and L. H. Chen, *Journal of Fujian Normal University*, 2014.
26. Y. D. Lu, X. X. Chen and L. H. Chen, *Applied Mechanics & Materials*, 2013, **395-396**.
27. G. Giallongo, R. Pilot, C. Durante, G. A. Rizzi, R. Signorini, R. Bozio, A. Gennaro and G. Granozzi, *Plasmonics*, 2011, **6**, 725-733.
28. G. Kartopu, M. Es-Souni, A. V. Sapelkin and D. Dunstan, *Physica Status Solidi Applied Research*, 2006, **203**, R82–R84.
29. Q. K, L. H, Y. L and L. J, *Nanoscale*, 2012, **4**, 6449-6454.
30. B. Mondal and S. K. Saha, *Chemical Physics Letters*, 2010, **497**, 89–93.
31. L. CH, T. L, A. A, K. R and S. S., *Nanotechnology*, 2011, **22**, 2593-2598.
32. M. Baibarac, M. Cochet, M. Łapkowski, L. Mihut, S. Lefrant and I. Baltog, *Synthetic Metals*, 1998, **96**, 63–70.
33. P. Nielsen, S. Hassing, O. Albrektsen, S. Foghmoes and P. Morgen, *J. Phys. Chem. C*, 2009, **113**, 14165-14171.
34. D. Choi, Y. Choi, S. Hong, T. Kang and L. P. Lee, *Small*, 2010, **6**, 1741–1744.
35. G. Das, N. Patra, A. Gopalakrishanan, R. P. Zaccaria, A. Toma, S. Thorat, E. D. Fabrizio, A. Diaspro and M. Salerno, *Microelectronic Engineering*, 2012, **97**, 383–386.
36. K. Malek, A. Brzózka, A. Rygula and G. D. Sulka, *Journal of Raman Spectroscopy*, 2014, **45**, 281–291.
37. S.-C. Luo, K. Sivashanmugan, J.-D. Liao, C.-K. Yao and H.-C. Peng, *Biosens Bioelectron*, 2014, **61**, 232–240.
38. A. Kudelski, *Chemical Physics Letters*, 2005, **414**, 271–275.
39. A. Campion, J. E. Ivanecky, C. M. Child and M. Foster, *J. Am. Chem. Soc.*, 1995, **117**, 11807-11808.
40. J. C. Bian, Z. D. Chen, Z. Li, F. Yang, H. Y. He, J. Wang, J. Z. Y. Tan, J. L. Zeng, R. Q. Peng and X. W. Zhang, *Applied Surfaceence*, 2012, **258**, 6632-6636.
41. T. T. B. Quyen, W.-N. Su, K.-J. Chen, C.-J. Pan, J. Rick, C.-C. Chang and B.-J. Hwang, *Journal of Raman Spectroscopy*, 2013, **44**, 1671–1677.
42. S. H. Ciou, Y. W. Cao, H. C. Huang, D. Y. Su and C. L. Huang, *Journal of Physical Chemistry C*, 2009, **113**, 9520-9525.
43. J. R. Kirtley, S. S. Jha and J. C. Tsang, *Solid State Communications*, 1980, **35**, 509–512.
44. P. Johansson, H. Xu, M. K, auml and ll, *Phys. Rev. B 72, 035427 (2005).* 2005.
45. H. J. Oh, G. S. Park, J. G. Kim, Y. Jeong and C. S. Chi, *Materials Chemistry & Physics*, 2003, **82**, 331–334.
46. D. Shan, L. Huang, X. Li, W. Zhang, J. Wang, L. Cheng, X. Feng, Y. Liu, J. Zhu and Y. Zhang, *J.phys.chem.c*, 2014.
47. D. Choi, Y. Choi, S. Hong, T. Kang and L. P. Lee, *Small*, 2010, **6**, 1741–1744.
48. R. Li, Q. W. Chen, H. Zhang, X. K. Kong, Y. B. Sun, H. Zhong, H. Wang and S. Zhou, *Journal of Raman Spectroscopy*, 2013, **44**, 525–530.